blood advances

American Society of Hematology
2021 L Street NW, Suite 900,
Washington, DC 20036
Phone: 202-776-0544 | Fax 202-776-0545
bloodadvances@hematology.org

CBFA2T3::GLIS2 Pediatric Acute Megakaryoblastic Leukemia is Sensitive to BCL-X_L Inhibition by Navitoclax and DT2216

Tracking no: ADV-2022-008899R2

Verena Gress (Faculty of Medicine, Université de Montréal, Montréal, Canada) Mathieu Roussy (Faculty of Medicine, Université de Montréal, Montréal, Canada) Luc Boulianne (CHU Sainte-Justine Research Center, Canada) Mélanie Bilodeau (CHU Sainte-Justine Research Center, Canada) Sophie Cardin (CHU Sainte-Justine Research Center, Canada) Nehme EL-Hachem (CHU Sainte-Justine Research Center, Canada) Véronique Lisi (Centre Hospitalier Universitaire Sainte-Justine Research Center, Canada) Banafsheh Khakipoor (CHU Sainte-Justine Research Center, Canada) Alexandre Rouette (Integrated Centre for Pediatric Clinical Genomics, CHU Sainte-Justine Research Center, Canada) Azer Farah (Centre Hospitalier Universitaire Sainte-Justine Research Center, Canada) Louis Théret (IRIC - University of Montreal, Canada) Léo Aubert (IRIC - University of Montreal, Canada) Furat Fatima (Department of Pathology, McGill University, Montréal, Canada) Eric Audemard (University of Montreal, Canada) Pierre Thibault (Universite de Montreal, Canada) Éric Bonneil (IRIC-Université de Montréal, Canada) Jalila Chagraoui (IRIC, Canada) Louise Laramée (CHU Sainte-Justine Research Center, Canada) Patrick Gendron (Université de montréal, Canada) Loubna Jouan (CHU Sainte-Justine Research Center, Canada) Safa Jammali (CHU Sainte-Justine Research Center, Canada) Bastien Paré (CHU Sainte-Justine Research Centre, Canada) Shawn Simpson (CHU Sainte-Justine Research Center, Canada) Thai Hoa Tran (Faculty of Medicine, Université de Montréal, Montréal, Canada) Michel Duval (Faculty of Medicine, Université de Montréal, Montréal, Canada) Pierre Teira (Faculty of Medicine, Université de Montréal, Montréal, Canada) Henrique Bittencourt (Faculty of Medicine, Université de Montréal, Montréal, Canada) Raoul Santiago (Centre hospitalier de l'Université Laval, Canada) Frédéric Barabé (Université Laval, Canada) Guy Sauvageau (Faculty of Medicine, Université de Montréal, Montréal, Canada) Martin Smith (Department of Biochemistry and Molecular Medicine, Faculty of Medicine, Université de Montréal, Quebec, Canada) Josée Hébert (Faculty of Medicine, Université de Montréal, Montréal, Canada) Philippe Roux (IRIC - University of Montreal, Canada) Tanja Gruber (Stanford University, United States) Vincent-Philippe Lavallée (Faculty of Medicine, Université de Montréal, Montréal, Canada) Brian Wilhelm (IRIC, Canada) Sonia Cellot (Faculty of Medicine, Université de Montréal, Montréal, Canada)

Abstract:
Acute megakaryoblastic leukemia (AMKL) is a rare, developmentally restricted and highly lethal cancer of early childhood. The paucity and hypocellularity (due to myelofibrosis) of primary patient samples hamper the discovery of cell- and genotype-specific treatments. AMKL is driven by mutually exclusive chimeric fusion oncogenes in two thirds of cases, with CBFA2T3::GLIS2 (CG2) and NUP98 fusions (NUP98r) representing the highest fatality subgroups. We established CD34+ cord blood-derived CG2 models (n=6) that sustain serial transplantation and recapitulate human leukemia regarding immunophenotype, leukemia initiating cell frequencies, co-mutational landscape and gene expression signature with distinct upregulation of the pro-survival factor BCL2. Cell membrane proteomic analyses highlighted CG2 surface markers preferentially expressed on leukemic cells compared to CD34+ cells (e.g. NCAM1, CD151). AMKL differentiation block in the mega-erythroid progenitor space was confirmed by single cell profiling. While CG2 cells were rather resistant to BCL2 genetic knockdown or selective pharmacological inhibition with Venetoclax, they were vulnerable to strategies that target the megakaryocytic pro-survival factor BCL-XL (BCL2L1), including in vitro and in vivo treatment with BCL2/BCL-XL/BCL-W inhibitor Navitoclax and DT2216, a selective BCL-XL PROTAC (proteolysis-targeting chimera) degrader developed to limit thrombocytopenia in patients. NUP98r AMKL were also sensitive to BCL-XL inhibition, but not the NUP98r monocytic leukemia, pointing to a lineage-specific dependency. Navitoclax or DT2216 treatment in combination with low dose cytarabine further reduced leukemic burden in mice. This work extends the cellular and molecular diversity set of human AMKL models and uncovers BCL-XL as a therapeutic vulnerability in CG2 and NUP98r AMKL.

Conflict of interest: No COI declared

COI notes:

Preprint server: No;

Author contributions and disclosures: V.G. and M.R. designed and performed the experiments, analyzed the data, generated the figures and wrote the manuscript. M.B. and S. Cardin led projects, performed experiments, analysed data and wrote the manuscript. L.B., L.L. and F.F. assisted with experiments and data collection. N.E.H. performed bioinformatic analysis, generated figures and wrote the manuscript. A.R., E.A., P.G., L.J., S.J. performed bioinformatic analysis. V.L., B.K., and A.F. performed and analysed scRNAseq analysis and wrote the manuscript. V.P.L. supervised bioinformatics and single cell experiments and analyses and wrote the corresponding manuscript sections. L.T., L.A. and P.P.R. performed and analysed the cell surface proteomic experiments. E.B. performed mass spectrometry analysis. B.P. and S.M.S. performed nanopore genome sequencing and bioinformatic analysis under the supervision of M.A.S. T.A.G. shared the AMKL validation cohort dataset. T.H.T., R.S., M.D., H.B., P. Teira, V.P.L. and S. Cellot oversaw patients and contributed to the biobanking. J.H. supervised the biobanking of patient specimens at the BCLQ. J.C., G.S., F.B., B.T.W., P. Thibault, H.B. provided guidance in designing the experiments and analyses. S. Cellot conceived the experiments, supervised the biobanking of patient specimens at the BCLQ, and wrote the manuscript. All authors reviewed the manuscript.

Non-author contributions and disclosures: No;

Agreement to Share Publication-Related Data and Data Sharing Statement: The RNAseq dataset was deposited in the Gene Expression Omnibus database (accession number GSE209628).

Clinical trial registration information (if any):

CBFA2T3::GLIS2 Pediatric Acute Megakaryoblastic Leukemia is Sensitive to BCL-X_L Inhibition by Navitoclax and DT2216

Verena Gress[1,2]*, Mathieu Roussy[1,2]*, Luc Boulianne[1,3], Mélanie Bilodeau[1], Sophie Cardin[1], Nehme El-Hachem[1], Véronique Lisi[1], Banafsheh Khakipoor[1], Alexandre Rouette[4], Azer Farah[1], Louis Théret[5], Léo Aubert[5], Furat Fatima[1,3], Éric Audemard[5], Pierre Thibault[5], Éric Bonneil[5], Jalila Chagraoui[6], Louise Laramée[1], Patrick Gendron[5], Loubna Jouan[4], Safa Jammali[4], Bastien Paré[1], Shawn M. Simpson[1], Thai Hoa Tran[1,2], Michel Duval[1,2], Pierre Teira[1,2], Henrique Bittencourt[1,2], Raoul Santiago[7], Frédéric Barabé[8,9], Guy Sauvageau[2,6,10], Martin A. Smith[1,11], Josée Hébert[2,12], Philippe P. Roux[2,5,13], Tanja A. Gruber[14,15], Vincent-Philippe Lavallée[1,2#], Brian T. Wilhelm[5#] and Sonia Cellot[1,2#]

1. Pediatric Hematology-Oncology division, Charles-Bruneau Cancer Center, CHU Sainte-Justine Research Center, Montréal, Québec, Canada; 2. Faculty of Medicine, Université de Montréal, Montréal, Québec, Canada; 3. Department of Pathology, McGill University, Montréal, Québec, Canada; 4. Integrated Centre for Pediatric Clinical Genomics, CHU Sainte-Justine Research Center, Montréal, Québec, Canada; 5. Institute for Research in Immunology and Cancer, Université de Montréal, Montréal, Québec, Canada; 6. Molecular Genetics of Stem Cells Laboratory, Institute for Research in Immunology and Cancer; 7. Division of Hematology-Oncology, Centre Hospitalier Universitaire de Québec-Université Laval (CHUL), Québec City, QC, Canada. 8. Centre de recherche du CHU de Québec-Université Laval, Québec, Canada; 9. Department of Medicine, Faculty of Medicine of Université Laval, Québec, Canada; 10. Division of Hematology, Maisonneuve-Rosemont Hospital, Montréal, Québec, Canada; 11, Department of Biochemistry and Molecular Medicine, Faculty of Medicine, Université de Montréal, Quebec, H3T 1J4, Canada. 12. Division of Hematology-Oncology and Quebec Leukemia cell bank, Hôpital Maisonneuve-Rosemont, Montréal, Québec, Canada; 13. Department of Pathology and Cell Biology, Faculty of Medicine, Université de Montréal, Montréal, Québec, Canada. 14. Department of Pediatrics, Stanford University School of Medicine, Stanford, California, USA; 15. Stanford Cancer Institute, Stanford University School of Medicine, Stanford, California, USA.

*These authors contributed equally to this work
# These authors shared senior authorship

Short title: AMKL is sensitive to BCL-X_L inhibition
text word count: 3999
abstract word count: 246
# of figures: 7
# of tables: 13
# of references: 67
Scientific category: Myeloid neoplasia

Corresponding author:
Sonia Cellot, CHU Sainte-Justine, 3175 Côte Sainte-Catherine, room 6-17-007, Montréal, Québec, Canada, H3T 1C5. Phone: (514)-345-4931 ext.6026. Fax: (514)-345-4884.
E-mail: sonia.cellot@umontreal.ca

The RNAseq dataset was deposited in the Gene Expression Omnibus database (accession number GSE209628). Contact the corresponding author for other forms of data sharing: sonia.cellot@umontreal.ca.

ABSTRACT

Acute megakaryoblastic leukemia (AMKL) is a rare, developmentally restricted and highly lethal cancer of early childhood. The paucity and hypocellularity (due to myelofibrosis) of primary patient samples hamper the discovery of cell- and genotype-specific treatments. AMKL is driven by mutually exclusive chimeric fusion oncogenes in two thirds of cases, with CBFA2T3::GLIS2 (CG2) and NUP98 fusions (NUP98r) representing the highest fatality subgroups. We established CD34+ cord blood-derived CG2 models (n=6) that sustain serial transplantation and recapitulate human leukemia regarding immunophenotype, leukemia initiating cell frequencies, co-mutational landscape and gene expression signature with distinct upregulation of the pro-survival factor BCL2. Cell membrane proteomic analyses highlighted CG2 surface markers preferentially expressed on leukemic cells compared to CD34+ cells (e.g. NCAM1, CD151). AMKL differentiation block in the mega-erythroid progenitor space was confirmed by single cell profiling. While CG2 cells were rather resistant to BCL2 genetic knockdown or selective pharmacological inhibition with Venetoclax, they were vulnerable to strategies that target the megakaryocytic pro-survival factor BCL-X_L (*BCL2L1*), including *in vitro* and *in vivo* treatment with BCL2/BCL-X_L/BCL-W inhibitor Navitoclax and DT2216, a selective BCL-X_L PROTAC (proteolysis-targeting chimera) degrader developed to limit thrombocytopenia in patients. NUP98r AMKL were also sensitive to BCL-X_L inhibition, but not the NUP98r monocytic leukemia, pointing to a lineage-specific dependency. Navitoclax or DT2216 treatment in combination with low dose cytarabine further reduced leukemic burden in mice. This work extends the cellular and molecular diversity set of human AMKL models and uncovers BCL-X_L as a therapeutic vulnerability in CG2 and NUP98r AMKL.

KEY POINTS

1. Cord blood–derived CBFA2T3::GLIS2 high-fidelity AMKL models contribute to capture the cellular and molecular heterogeneity of the disease
2. BCL-X_L inhibition is revealed as a therapeutic vulnerability in CG2 and NUP98r AMKL

INTRODUCTION

Acute megakaryoblastic leukemia (AMKL) is a developmentally restricted and early-onset cancer affecting children 0-4 years of age, including neonates[1-4], pointing to a stem or progenitor cell of origin that is only transiently present in time[5]. It represents ~10% of pediatric acute myeloid leukemia (AML) cases and is a molecularly heterogenous and highly lethal leukemia, with dismal cure rates (<50%)[6]. Two-thirds of AMKL cases are driven by mutually exclusive chimeric fusion oncogenes including *RBM15::MKL1*[7,8], *KMT2A* translocations[9], and cytogenetically cryptic rearrangements involving either *NUP98*[10,11] (NUP98r, specifically *NUP98::KDM5A* (N5A)[12] and *NUP98::BPTF* (NTF)[13]), *HOX* genes[1,2,9] or the *CBFA2T3::GLIS2* (CG2) fusion[14-18]. The mapping of functional dependencies of *de novo* pediatric AMKL is emerging[19,20], and a repertoire of relevant preclinical models is needed to develop cell- and genotype-specific treatments for pediatric leukemia patients.

CG2 and NUP98r AMKL are recognised as the highest relapse risk subgroups [6,16,21]. The CG2 fusion results from a cryptic inversion on chromosome 16, joining the N-terminal nervy homology regions (NHR2, protein-interacting domains) of co-repressor *CBFA2T3* (*ETO2*) to the C-terminal zinc finger domains of transcription factor *GLIS2*, which allows binding to *GLI* DNA consensus sequences[14,15]. CBFA2T3 is involved in hematopoietic stem cell (HSC) maintenance and differentiation, as well as in the regulation of erythro-megakaryocytic progenitors[22-24]. GLIS2 was primarily identified in adult kidneys, maintaining normal tissue architecture and function[25]. CG2-targeting treatments are actively explored, including Aurora A kinase

inhibitors[14,26], interference with CG2 fusion oligomerization[27], targeting of cell adhesion molecule NCAM1[17], the FOLR1 receptor[18,28], or the JAK-STAT pathway with Ruxolitinib[12,29].

Resisting cell death is a long-recognised hallmark of cancer[30], and agents that promote apoptosis entered the therapeutic arena for AML[31]. The subsequent development of pharmacological inhibitors (BH3 mimetics) that target single or multiple pro-survival proteins[32,33] has sparked significant interest in oncology as these agents can induce mitochondrial apoptosis in multiple hematological malignancies[34,35] with significant clinical responses[36], including in children[37,38]. Evidence suggests that pro-survival factor dependency is both lineage-[39-42] and mutation-specific[43,44] in leukemia, and the integration of BH3 mimetics into current treatment protocols is under active investigation.

To define AMKL functional dependencies and overcome the paucity of pediatric patient samples, we have engineered CG2 AMKL models derived from cord blood (CB) hematopoietic stem and progenitor cells (HSPC) that phenocopy the human disease. Across AMKL genotypes, CG2 leukemia distinctively upregulate the pro-survival factor BCL2 yet are resistant to BCL2-specific inhibition with Venetoclax or genetic knockdown. In contrast, targeting the megakaryocytic lineage pro-survival factor BCL-X_L[45,46] with Navitoclax[47] (binding to BCL2, BCL-X_L and BCL-W) or BCL-X_L proteasomal degrader DT2216[48] induced apoptosis of CG2 and NUP98r AMKL cells, with minimal cross toxicity on normal CB-CD34+ HSPC. Our work highlights pro-survival protein BCL-X_L as a therapeutic vulnerability in pediatric AMKL and is timely aligned with a recent study suggesting that BCL-X_L is also a potential target of adult mega-erythroid

leukemia[49]. Addition of anti-BCL-X_L agents to cytarabine-based chemotherapy regimens in pediatric AMKL clinical trials is within reach and not exploited.

METHODS

Extended methods are provided in supplemental methods.

Patient samples

Pediatric AMKL samples (Table S1 and [12]) were collected with approval from the Research Ethics Boards (REB) of Centre Hospitalier Universitaire (CHU) Sainte-Justine and informed patient consent in agreement with the Declaration of Helsinki. Biobanking was overseen by the Quebec Leukemia Cell Bank (Montreal, Canada).

Generation of CG2 models

CBFA2T3::GLIS2 cDNA was amplified from M07e cell line and cloned into the MNDU lentiviral expression vector (Table S2). Umbilical cord blood units, collected with maternal consent, were distributed by Héma-Québec (Montréal, Canada) and manipulated as described[12]

Xenotransplantation

Mouse experimental procedures were performed in accordance with the Canadian Council of Animal Care and with approval from the CHU Sainte-Justine REB and Animal Institutional Ethic

Committee (approval number: MP-21-2017-1566). Xenotransplantation and characterization protocols are provided in the suppl. methods.

Flow cytometry

Immunophenotyping antibodies are listed in Table S3. Apoptotic assays and intracellular staining are detailed in suppl. methods.

Molecular studies

Detailed protocols and sample descriptions are presented in suppl. methods and Table S4.

RNA sequencing. RNA sequencing (RNAseq) and data processing were performed at the Institute for Research in Immunology and Cancer's Genomics Platform (Montreal, Canada) using the Illumina Nextseq500 with 150 cycles paired-end runs. Sequences were aligned to the reference human genome version GRCh38.

Single cell RNA sequencing. Single cell suspensions were processed on the Chromium Controller according to manufacturer's protocol and sequenced at the CHU Sainte-Justine Integrated Centre for pediatric clinical genomics (Montreal, Canada).

***In vitro* pharmacological inhibition assays**

Synthetic models were maintained in optimised serum-free media. Navitoclax (ABT-263), Venetoclax (ABT-199), DT2216, cytarabine (AraC) and Staurosporine were purchased from

MedChemExpress (NJ, USA). Media composition, dose response curves and functional assays are described in suppl. methods.

In vivo drug studies

AMKL-xenotransplanted mice were treated either daily by oral gavage with Navitoclax (100mg/kg, ABT-263[47]), DT2216 i.p. every 4 days (15mg/kg)[48] or vehicle only. For drug combinations, mice were additionally treated with cytarabine (AraC, 20mg/kg, i.p.) for the first 5 days. Detailed protocols are described in suppl. methods.

Data Sharing Statement

The RNAseq dataset was deposited in the Gene Expression Omnibus database (accession number GSE209628).

RESULTS

CG2 gene fusion transforms CD34+ cord blood cells

To generate human leukemia models, we overexpressed CG2 in pooled CB-CD34+ purified cells by transduction with a lentiviral construct carrying the fusion oncogene and a GFP reporter (Fig.1A). Gene transfer rates averaged 12.5% (Fig.1B) and 80% of each well was separately transplanted into one NSG recipient mouse. Leukemia penetrance was of 60% with latencies between 9.9 to 36.1 weeks (Fig.1B). Expression of the CG2 fusion transcript was confirmed by RT-PCR analysis (Fig.1C) and RNA sequencing of leukemic cells. Expression levels of the CG2 fusion transcript and wild type *CBFA2T3* were comparable between models and patient

samples (Suppl.Fig.S8). At necropsy of leukemic mice, infiltration of hematopoietic organs by leukemic blasts was confirmed in bone marrow (BM) and spleen (hCD45+GFP+ cells, Fig.1D-F, Suppl.Fig.S1, Table S5). No adverse outcomes were documented in the empty-vector control group (n=10, Fig.1F-G). All six engineered leukemic models were able to robustly sustain serial transplantation with consistent disease phenotype and latencies (~8-12 weeks), tested for up to 4 passages *in vivo* (Fig.1G, Suppl.Fig.S1, Table S5). As seen in CG2 patients, some mice exhibited neurological deficits of variable intensities indicative of leukemic paraspinal infiltration, which was confirmed by bioluminescent imaging of luciferase-transduced grafts (Suppl.Fig.S2).

The generated leukemia showed megakaryocytic morphology and lineage markers (hCD45+CD34+/-CD41+CD61+) with significant CD56 (NCAM1) expression, a hallmark of CG2 AMKL[14,15,50] (Fig.1H-K, Suppl.Fig.S4, Table S5). The CG2-6 model was hCD45+CD71+CD117+ by immunophenotyping, with lower surface expression of CD41 (Fig.1E), CD34, CD33, CD56 and absence of myelo-monocytic markers (MPO, CD68, LYZ, FUT4/CD15 and ITGAM/CD11b) by transcriptomic and flow cytometry (Table S5, Suppl.Fig.S3-4), pointing to an early mega-erythroid progenitor state. AMKL development *in vivo* was retained after *in vitro* culture for 6 days, providing physiologically relevant cellular substrate for biochemical analyses (Suppl.Fig.S5)

AMKL leukemia initiating cell (LIC) frequency was assessed by limiting dilution assay (LDA) using cells isolated from mCG2-1, mCG2-2 and mCG2-6 recipients and approximated 1 in 3,400 cells, 1 in 14,938 cells, and 1 in 15,286 cells, respectively, close to the 1 in 10,300 LIC frequency

assessed in a NUP98r patient sample (Fig.1L-M, Table S6). Time to overt leukemia was proportional to cell dose, with 4 of 8 mice of mCG2-1 succumbing to AMKL 20-30 weeks after injection of 250 cells (Fig.1L, Table S6). Overall, the engineered CG2 AMKL faithfully recapitulate human disease, reside in the mega-erythroid differentiation space and harbor high LIC frequencies, as reported for patient samples[14].

AMKL CG2 models phenocopy human disease at the molecular level

Transcriptomic profiling of the CG2 models closely correlate with genotype-matched patient samples (r=0.64; n=2, institutional cohort; n=12, validation cohort[9], Fig.2A), with high expression of *NCAM1*, *BMP2*, *ERG* and low *GATA1* levels[5,14,15,27]. A CG2-specific gene signature of up- and downregulated markers was derived by comparing the expression profiles of CG2 models and patients (n=10) against institutional NUP98r AMKL (n=7) and CB-CD34+ cells (n=4), cross-validated in a patient cohort comprising different AMKL genotypes[9] (n=73 total, with n=12 CG2) (Fig.2A, Table S7). CG2 AMKL is a non-HOXA/B, non-MEIS1/2 leukemia, which distinctively expresses *GLIS2*, whereas *CBFA2T3* is expressed across AMKL genotypes (Suppl.Fig.S6B). Remarkably, CG2 AMKL upregulated pro-survival factor *BCL2* (Fig.2A), pointing to a potential subtype-specific vulnerability. Furthermore, the engineered CG2 AMKL models cluster with CG2 patients (n=14) by expression profiling (Fig.2B) and apart from other AMKL genotypes and CB-CD34+ cells. Principal component analysis revealed clustering of primary and tertiary xenografts based on expression profile (Suppl.Fig.S6A).

Akin to patient samples[2,9,15], the genomic landscape of the engineered CG2 models was rather silent as assessed by whole exome sequencing (WES) and comparative genomic hybridization (CGH) (Suppl.Fig.7), with no recurrent co-operating mutations, pathogenic single nucleotide variants (SNV) or indels. Comparable to the reported genomic landscape of human disease[15], copy number variations (CNV) were identified in 4 of the 6 models, and chromosomal alterations remained stable over serial transplantation for two models analysed (Suppl.Fig.S7). We excluded insertional mutagenesis events by long-read DNA sequencing (n=4) and confirmed the (oligo)-clonal character of the engineered AMKL models (Suppl.Fig.S9). The CG2 AMKL models thus transcriptionally phenocopy human disease and appear genetically stable through serial transplantation.

Proteomic analyses of human CG2 models identify genotype-specific surface markers

We used a surface proteome (surfaceome) approach, as previously described[12,51-53], to identify CG2-specific membrane proteins vs normal HSPC (n=11 CB-CD34+, n=2 CG2 AMKL and n=2 NUP98r AMKL[12,13]) (Fig.2C, Suppl.Fig.S10, Table S9). Comparing proteomic datasets of CG2 and CB-CD34+ cells confirmed that CG2 models express AMKL-associated markers CD151[54], ITGA2B, PECAM1 (CD31[55] and NCAM1 (CD56)[14,15,17] (Suppl.Fig.S10E). The 25 most abundant and differentially expressed proteins in CG2 vs CB-CD34+ were cross-validated against an external AMKL patient transcriptomic dataset[9] (Fig.2C, Suppl.Fig.S11B). Eight of these markers (CSF2RA, DPP10, NCAM1, NRP1, PCDH10, PCDH19, RECK, SCN9A) were significantly associated with the CG2 genotype (highlighted in S11B and Fig.2D). Five of the 25 surfaceome proteins could be validated using available flow cytometry antibodies, showing that PCDH19 and JAG1 were

detected on a subset of cells across all patients and models, while CSF2RA, NRP1 and INSR were only detected in a subset of samples (Fig.2E, Suppl.Fig.S12). Similarly, the FOLR1 receptor, recently reported to be associated with CG2 AMKL[18], was found to be expressed on a significant proportion of cells across models, except for mCG2-6. Of note, the CD41^{low} CG2-6 cells express CD31/CD151 but upregulate CD41/CD61 in culture (Suppl.Fig.S4), pointing to immature leukemic cells that are primed towards the megakaryocytic lineage. Pairwise correlation analyses of cell surface markers most associated with CG2, uncovered that the combination of *NCAM1* with either *PCDH10* or *PCDH19* was most predictive of the CG2 genotype (Fig.2F, Suppl.FigS13, Table S10, p-val. <0.05). These markers can contribute to refine the panel of markers used for CG2 AMKL diagnosis and tracking of minimal residual disease (MRD) in patients[56].

CG2 leukemia lie in the mega-erythroid stem and progenitor differentiation space

Engineered CG2 models (n=4) and patients (n=2) were profiled by single-cell RNA sequencing (scRNAseq) to determine their cellular composition (Fig.3, Suppl.Fig.S14-S17). Key upregulated genes of normal megakaryocyte-erythroid progenitors (MEP), megakaryocyte progenitors (MKP) and platelets were inferred from normal BM cell populations (Human Cell Atlas, HCA[57], Fig.3A-B, Table S11). MEP/MKP/platelet-specific genes, e.g. *ITGA2B* (CD41), are universally expressed in CG2 AMKL cells but not in adult AML cells[58] (Fig.3C, Suppl.Fig.S15-S16). The MKP-specific genes *GP1BA* (Glycoprotein 1B Platelet subunit alpha, CD42b) and *GP9* (Glycoprotein IX)

are more expressed in CG2 than normal MEP cells, indicating that CG2 leukemic cells lie towards the primitive megakaryocytic differentiation space. Transferring the cell type assignment from the HCA to AMKL and AML datasets, confirmed the dominant MKP bias of CG2 models and patients compared to other AML samples (grey shaded samples in Fig.3D, upper panel, Suppl.Fig.S14B-C). CG2 AMKL samples contain varying MEP proportions (Fig.3D lower panel), with the CG2-6 model partially projecting into the erythroid space (Fig.3D, blue shading in radar plot, CD34+ ERP fractions in lower panel). While MKP genes are homogeneously expressed in CG2 samples, only small subsets express genes suggesting terminal differentiation such as *CLEC1B* (Fig.3E, Suppl.Fig.S15-S16). This data indicates that CG2 models reside predominantly in the MKP differentiation space and recapitulate the lineage commitment of CG2 AMKL patients.

Co-embedding the datasets in the same UMAP revealed that CG2 models and patients lie in an area of the UMAP representation also populated by normal BM cells (HCA) of the megakaryocytic lineage (Suppl.Fig.S17A), highlighting the low inter-sample heterogeneity, in contrast to the large cell heterogeneity of normal BM, as seen by the distribution overlap of the CG2 models and patients (Suppl.Fig.S17B).

Furthermore, gene expression of leukemic CG2 MKP was compared to normal MKP to identify aberrantly expressed genes, such as *NCAM1* and *BCL2* (Fig.3F-G, Table S12), mirroring the CG2 bulk transcriptomic signature (Fig.2A). While no other BCL2 family member was aberrantly expressed in CG2 MKP, *BCL2L1* (BCL-X_L) is specifically expressed in normal MEP/MKP/platelet

subsets as compared to other cell types (adj. p-val=7.5 x 10^{-111}, Fig.3B, Suppl.Fig.S14E), and *BCL2L1* expression is maintained across CG2 models and patients (Fig.3G, Suppl.Fig.S15-S16). This provides a rationale to assess the functional dependency of CG2 cells to BCL-X_L, based on lineage ontogeny, and to BCL2, given its aberrant expression in CG2 AMKL.

AMKL cells are resistant to Venetoclax but sensitive to Navitoclax

We tested sensitivity of AMKL cells to BCL2 inhibitor Venetoclax (CG2 n=6, N5A n=2[12], pdxNTF n=1[13],) as well as in AML samples (MLLr n=2, NNSD1 n=1 and N5A monocytic (CD68+LYZ+) AML models n=2[12]). All AMKL samples tested were resistant to Venetoclax with IC50s (half maximal inhibitory concentration) >10μM whereas AML samples were sensitive to Venetoclax (Fig.4A, Table S13). In contrast, both CG2 and NUP98r AMKL were sensitive to Navitoclax, which has a broader affinity to BCL2, BCL-X_L, and BCL-W, as well as AML samples (Fig.4B, Table S13), while genotype-matched monocytic N5A AML cells were resistant, suggesting a lineage-specific vulnerability. AMKL cells exposed to Navitoclax for 72hrs at concentrations spanning the leukemia-specific IC50 values exhibited higher levels of apoptosis than control CB-CD34+ cells (Fig.4C). In contrast, exposure to Venetoclax did not induce apoptosis in AMKL cells at doses up to 10μM (Fig.4D). Levels of mitochondrial superoxide radicals and loss of mitochondrial potential were higher in AMKL cells treated with Navitoclax than cells treated with Venetoclax (Fig.4E-F, Suppl.Fig.S18A), suggesting mitochondrial dysfunction. These results imply that AMKL cells are sensitive to BCL2/BCLX_L/BCL-W inhibitor Navitoclax with subsequent induction of mitochondrial apoptosis, yet resistant to Venetoclax that uniquely targets BCL2.

Inhibition of BCL-X_L induces mitochondrial apoptosis of CG2 and NUP98r AMKL

To dissect whether the induction of apoptosis in AMKL cells by Navitoclax is mediated via BCL2, BCL-X_L or BCL-W inhibition, expression levels of each gene were assessed using transcriptomic datasets. In accordance with the CG2 signature (Fig.2A), *BCL2* was most abundant in CG2 compared to NUP98r AMKL cells (institutional cohort, Fig.5A) and all other AML genotypes (n=7 CG2, n=73 patients total, validation cohort[9]) (Fig.5B). In contrast, *BCL2L1* (BCL-X_L) is homogenously expressed across AMKL genotypes and at much lower levels in the N5A monocytic AML (n=3). Intracellular protein levels of BCL-X_L were correspondingly increased in CG2 and NUP98r AMKL as compared to normal CB-CD34+ cells, while the BCL2 protein was only detected in the CG2 genotype, matching mRNA expression (Fig.5C). Sh-mediated knock-down (KD) against *BCL2*, *BCL2L1* or *BCLW* was used to assess the functional impact of reduced pro-survival factors in two distinct CG2 models (gene transfer >95% GFP+mCherry+ cells, Fig.5D-E, Suppl.Fig.S18B-C), with confirmation of efficient protein reduction of BCL2 and BCL-X_L (Fig.5F, Suppl.Fig.S15D). Increased apoptosis of AMKL cells (AnnexinV+ cells, Fig.5D, Suppl.Fig.S15E) was observed only with KD of BCL-X_L, but not BCL2 or BCL-W. Additionally, AMKL and monocytic N5A AML models were treated with DT2216[48], a selective BCL-X_L proteolysis-targeting chimera (PROTAC) that targets BCL-X_L to the Von Hippel-Lindau E3 ligase (VHL) for degradation. VHL is abundantly expressed in our models of AMKL (Fig.5A) but not expressed in platelets, which are most vulnerable to BCL-X_L inhibition[48]. In a dose-response experiment, AMKL models were sensitive to DT2216 with IC50 concentrations below 200nM (Fig.5G, Table S13). In contrast, monocytic N5A AML models demonstrated resistance to DT2216 treatment with IC50 values above 10µM (Fig.5G, Table S13). AMKL cells exposed to 100nM and 1µM of DT2216 showed

significantly higher levels of apoptosis compared to normal CB-CD34+ cells (Fig.5H) and higher mitochondrial stress, shown by increased superoxide levels and loss of mitochondrial membrane potential (Suppl.Fig.S18F-G). Furthermore, testing Navitoclax, Venetoclax and DT2216 on several independent CB-CD34+ pools revealed sample-dependent variability in drug response but overall lower toxicity with DT2216 in comparison to Navitoclax (Suppl.Fig.S18H, Table S13). These results suggest that the sensitivity of AMKL cells towards Navitoclax is due to the inhibition of BCL-X_L, demonstrated by genetic and pharmacological inhibition.

Monotherapy with Navitoclax or DT2216 reduces leukemic burden in high-fatality AMKL *in vivo*

To investigate the *in vivo* impact of BCL-X_L inhibition of Navitoclax or DT2216 as single agent, three independent models of AMKL were tested (Fig.6A, Suppl.Fig.S19-20), as well as chemo-refractory PDX of NTF[13] (Suppl.Fig.S19-20). After a 3-week treatment cycle with Navitoclax, a significant reduction of leukemic infiltration was noted in mCG2-1, as assessed by spleen weight (Fig.6B) and abundance of GFP+hCD45+ AMKL cells in blood, BM and spleen (Fig.6C-D). Normal hematopoietic cell distribution and tissue architecture was restored in BM and spleen of Navitoclax-treated mice vs control (Fig.6E). Furthermore, Navitoclax-treated mice showed reduced circulating blasts during treatment (wk5) as well as one week after treatment (wk7, Fig.6F), conferring a survival benefit over vehicle-treated mice (Fig.6G). For mCG2-2, treatment was stopped early due to rapid onset of hindleg paralysis. Nevertheless, a significant reduction of overall leukemic burden was detected after 2 weeks of treatment, measured by luciferase intensity (Suppl.Fig.S19A-B), as well as reduction of GFP+Ametrine+ cells in the spleen in

comparison to vehicle controls (Suppl.Fig.S19C). Reduced leukemic progression was seen in pdxNTF-xenografted mice treated with Navitoclax by *in* vivo imaging which was significantly lower compared to vehicle control mice post treatment (wk8, Suppl.Fig.S19D-E).

We furthermore tested DT2216 in two distinct models of CG2 (mCG2-1 and mCG2-6), presenting either as megakaryopoietic or mega-erythroid leukemia, and in pdxNTF. Xenografted mice were treated with DT2216 every 4 days for a total of 4-6 weeks. Treatment with DT2216 demonstrated reduced leukemic blasts in the blood (GFP+hCD45+ cells, Fig.6H) and significantly prolonged survival of mCG2-1 transplanted mice in comparison to vehicle controls (Fig.6I). Mice transplanted with CG2-6 were investigated after 6 weeks of treatment by BM aspiration and showed significant reduction of hCD45+GFP+CD31+CD151+ leukemic cells in the BM in comparison to vehicle controls (Suppl.Fig.S20A-B). Additionally, a 4-week treatment cycle of DT2216 significantly reduced leukemic burden in pdxNTF-xenografted mice (Suppl.Fig.S20C). This work demonstrates that BCL-X_L degradation either with Navitoclax or DT2216 could be exploited as a strategy in the treatment of high-fatality CG2 and NUP98r AMKL.

Combinatorial use of Navitoclax or DT2216 with cytarabine has potent anti-AMKL activity *in vivo*.

Cytarabine is a standard of care (SOC) component of chemotherapy induction and intensification cycles for AML patients. In this context, combinatorial treatment with BCL-X_L inhibitors and cytarabine was tested in CG2 AMKL. First, all CG2 models showed sensitivity

towards cytarabine *in vitro* with IC50s ranging from 1 to 7nM (Fig.7A, Table S13). To assess the *in vivo* anti-leukemia activity of either Navitoclax or DT2216 combined with cytarabine, NSG mice were xenografted with mCG2-1 and treated with low-dose cytarabine (20mg/kg) for 5 consecutive days alongside Navitoclax or DT2216 (Fig.7B, Suppl.Fig.S21A). Engraftment was verified for all groups before treatment by bleeding 3 weeks post-transplant (Suppl.Fig.21B-C). At endpoint, mice treated with the combination of cytarabine and Navitoclax showed significantly lower leukemic infiltration the blood, BM and spleen as compared to single agent alone or vehicle control mice (Fig.7C). In monotherapy, Navitoclax or cytarabine performed equivalently in terms of leukemic burden reduction (Fig7C). The same *in vivo* response was observed following combinatorial treatment with DT2216 and cytarabine (Suppl.Fig.21D). Of note, although Navitoclax shows a steeper reduction of leukemic burden as a single agent in comparison to DT2216, treatment of either Navitoclax or DT2216 combined with cytarabine was equally effective against CG2 AMKL (Fig.7E, Suppl.Fig.21F). These results highlight the translational potential of combining SOC cytarabine with BCL-X_L inhibitors in the treatment of high-fatality pediatric AMKL.

DISCUSSION

We bring forward six human models of CG2 AMKL that can sustain serial transplantation and phenocopy the clinical features, expression signature, genomic landscape, cellular ontogeny and high LIC frequencies of the disease. Progress in the field is hampered by limited patient samples currently available for preclinical testing, a restricted pool of representative cell lines and human models. Synthetic CG2 models contribute to map functional dependencies, capture

the cellular and molecular heterogeneity of the leukemia, maturation block, concomitant genetic alterations and surface marker expression. They represent faithful and scalable biomasses for biochemical studies, such as proteomics, to uncover new CG2 biomarkers that are either mega-erythroid lineage specific (CD151, PECAM1), distinct from normal CB progenitors (JAG1) or most predictive of the CG2 AMKL genotype (NCAM1, PCDH10, PCDH19), which can contribute to optimise flow cytometry antibody panels for CG2 AMKL diagnosis or MRD tracking.

Cell- and genotype-specific therapies are needed for pediatric AMKL to improve patient survival. Our models of CG2 highlight pro-survival factor BCL-X_L as a novel therapeutic target of high-fatality AMKL. *In vitro* pharmacological inhibition of BCL-X_L with Navitoclax or DT2216 induces apoptosis in all CG2 AMKL models, accompanied by mitochondrial dysfunction. This was recapitulated by genetic knockdown of BCL-X_L but not BCL2 or BCL-W, suggesting that CG2 AMKL depend preferentially on BCL-X_L to resist apoptosis. Similarly, NUP98r AMKL cells (n=3) were also sensitive to Navitoclax or DT2216 treatment, while genotype-matched monocytic AML were resistant, pointing to a lineage-specific dependency. Indeed, pro-survival factor dependencies are cell context-specific, with the megakaryocytic lineage relying predominantly on BCL-X_L [45,59,60] for proper maturation.

Importantly, following *in vivo* treatment with either Navitoclax or DT2216, we note a reduction in tumor burden and a survival benefit of leukemic mice, using three CG2 models (mCG2-1, 2 and 6) and a PDX of NUP98r AMKL, the two highest fatality AMKL subgroups. The mCG2-6

model resides in a distinct mega-erythroid differentiation space (CD41^{low}CD31+CD151+), reflecting the cellular heterogeneity of CG2 AMKL, yet demonstrates a common BCL-X_L dependency across this cellular context. Our findings are aligned with a recent publication reporting that adult leukemia of the mega-erythrocytic lineage are sensitive to BCL-X_L-specific inhibitor A-1331852, including the HEL erythrocytic line *in vivo*[49].

Expression of BCL2 on its own is not considered a predictor of drug response to Venetoclax[61] and may explain the relative resistance of CG2 leukemic cells to BCL2 inhibition, as suggested by our work and others[62,63]. An important finding, since Venetoclax (potent BCL2 inhibitor) is gaining unprecedented momentum for leukemia treatment[37,38], including in children. Given that CG2 cells do express higher baseline BCL2 levels than NUP98r AMKL and normal MEP-MKP, combinatorial strategies that trigger apoptosis such as cytotoxic or targeted chemotherapy, in addition to BCL2 inhibition, may ultimately induce apoptosis in CG2 cells that express BCL2, as recently suggested with either azacytidine[64] or MCL inhibitor S63845[62].

Moving forward, our work demonstrates that combining BCL-X_L inhibitors (Navitoclax or DT2216) and low-dose cytarabine is more potent against AMKL *in vivo* than either single agent alone, with significant translational potential given the current use of Venetoclax and high dose cytarabine in the treatment of relapsed or refractory pediatric AML[37,64,65]. However, thrombocytopenia is a dose-limiting toxicity of Navitoclax due to BCL-X_L inhibition in the megakaryocytic lineage[66]. Platelets express BCL-X_L at higher levels than MEP-MKP (Suppl.Fig.S16), in line with the rapid drop in platelets observed in patients exposed to

Navitoclax[67]. The BCL-X_L degrader DT2216, developed to mitigate the on-target thrombocytopenia of Navitoclax, interacts with the Von Hippel-Lindau E3 ligase which is weakly expressed in platelets. When gauging treatment toxicity on normal cells, we found that DT2216 was less toxic to CB-CD34+ cells as compared to Navitoclax, underscoring the translational potential of BCL-X_L degraders for treatment of hematological malignancies of the mega-erythrocytic lineages. Although monotherapy with Navitoclax may seem slightly more effective than DT2216 against AMKL *in vivo* (Fig.7D), the DT2216 intermittent dosing scheme can be further optimised in future studies, and importantly, both agents are equally effective in combination with cytarabine. Altogether, these preclinical studies suggest that integration of selective and potent BCL-X_L inhibitors to existing treatment regiments may improve disease eradication in pediatric AMKL.

ACKNOWLEDGEMENTS

The authors kindly thank the patients and their families and members of the pediatric Hematology-Oncology Team of CHU Sainte-Justine for their outstanding support; the members of the BCLQ and the Hematology-Oncology Division of CHU Sainte-Justine for their contribution to the biobanking initiative; Élie Haddad, Kathie Béland and the members of the humanized mouse core facility (CHU Sainte-Justine); Ines Boufaied of the flow cytometry facility (CHU Sainte-Justine) for cell sorting; Virginie Saillour, Charles Privé and René Allard of the Integrated Centre for pediatric clinical genomics at CHU Sainte-Justine for WES and scRNAseq studies; France Léveillé, Frédérique Tihy, Géraldine Mathonnet and Emmanuelle Lemyre of the Medical Genetics Service at CHU Sainte-Justine for CGH analysis; Elke Küster-Schöck of the microscopy facility at CHU Sainte-Justine; Raphaëlle Lambert from the Genomics Core Facility (Institute of Research in Immunology and Cancer, IRIC) for RT-qPCR and RNAseq analysis; Simon Mathien and Jean Duchaine from the High Throughput Screening Core Facility (IRIC) for dose-response experiments; Marianne Issac from the Histology Platform (IRIC) for processing of histological samples; Carolina Marmolejo, Anne-Cécile Soufflet, Emma Rose Cheetham, Nadia Emely Chauca Torres and Françoise Couture for their help with experiments; Sami Ayachi for bioinformatic analysis; Keith Humphries, Donald B. Kohn and Connie Eaves for providing lentiviral vectors; Michael A. Lieberman for offering the CHRF-288-11 cell line.

This study was supported by seminal Cole Foundation Transition Awards (S. Cellot and V.P.L.), Terry Fox Research Institute (TFRI) New Investigator grants, a Canadian Cancer Society Research Institute (CCSRI)/Cole Foundation Impact grant (S. Cellot and B.T.W.), an operating grant from

the Leukemia and Lymphoma Society of Canada (S. Cellot), an operating grant from the Richard and Edith Strauss Foundation (S. Cellot and B.T. W.), an operating grant from the Canadian Institutes of Health Research (S. Cellot and H.B.; FRN 178326), funding from the CHU Sainte-Justine Foundation (Fonds d'Innovation Thérapeutique), the Charles-Bruneau Foundation (operating grants), and the Canada Foundation for Innovation (John R. Evans Leaders Fund) (S. Cellot). This research work was made possible thanks to the financial support of the Oncopole, which receives funding from Merck Canada Inc., the Fonds de recherche du Québec – Santé (FRQS), Génome Québec, the Cancer Research Society and IRICoR (B.T.W., F.B., S. Cellot). V.P.L. is supported by a FRQS Junior 1 Clinical Research Scholarship and by the CHU Sainte-Justine and Charles-Bruneau Foundations. S. Cellot is recipient of a Clinician scientist senior award from the FRQS. V.G., M.R., N.E.H., B.K. and L.T. are recipients of Cole Foundation fellowships. NEH is supported by a post-doctoral Institut de valorisation des données (IVADO) scholarship. The Quebec Leukemia Cell Bank is supported by the Cancer Research Network of the FRQS. The humanized mouse core and the flow cytometry facilities at CHU Sainte-Justine are supported by the Charles-Bruneau Foundation.

AUTHORSHIP CONTRIBUTIONS

V.G. and M.R. designed and performed the experiments, analyzed the data, generated the figures and wrote the manuscript. M.B. and S. Cardin led projects, performed experiments, analysed data and wrote the manuscript. L.B., L.L. and F.F. assisted with experiments and data

collection. N.E.H. performed bioinformatic analysis, generated figures and wrote the manuscript. A.R., E.A., P.G., L.J., S.J. performed bioinformatic analysis. V.L., B.K., and A.F. performed and analysed scRNAseq analysis and wrote the manuscript. V.P.L. supervised bioinformatics and single cell experiments and analyses and wrote the corresponding manuscript sections. L.T., L.A. and P.P.R. performed and analysed the cell surface proteomic experiments. E.B. performed mass spectrometry analysis. B.P. and S.M.S. performed nanopore genome sequencing and bioinformatic analysis under the supervision of M.A.S. T.A.G. shared the AMKL validation cohort dataset. T.H.T., R.S., M.D., H.B., P. Teira, V.P.L. and S. Cellot oversaw patients and contributed to the biobanking. J.H. supervised the biobanking of patient specimens at the BCLQ. J.C., G.S., F.B., B.T.W., P. Thibault, H.B. provided guidance in designing the experiments and analyses. S. Cellot conceived the experiments, supervised the biobanking of patient specimens at the BCLQ, and wrote the manuscript. All authors reviewed the manuscript.

DISCLOSURE OF CONFLICTS OF INTEREST

The authors declare no conflict of interest.

REFERENCES

1. Gruber TA, Downing JR. The biology of pediatric acute megakaryoblastic leukemia. *Blood*. 2015;126(8):943-949.
2. Lopez CK, Malinge S, Gaudry M, Bernard OA, Mercher T. Pediatric Acute Megakaryoblastic Leukemia: Multitasking Fusion Proteins and Oncogenic Cooperations. *Trends Cancer*. 2017;3(9):631-642.
3. Bain BJ, Chakravorty S, Ancliff P. Congenital acute megakaryoblastic leukemia. *Am J Hematol*. 2015;90(10):963.
4. Messiaen J, Uyttebroeck A, Michaux L, Vandenberghe P, Boeckx N, Jacobs SA. t(1;7;22)(p13;q21;q13) is a novel 3-way variant of t(1;22)(p13;q13) neonatal acute megakaryoblastic leukemia: A case report. *Mol Clin Oncol*. 2023;18(3):18.
5. Lopez CK, Noguera E, Stavropoulou V, et al. Ontogenic Changes in Hematopoietic Hierarchy Determine Pediatric Specificity and Disease Phenotype in Fusion Oncogene-Driven Myeloid Leukemia. *Cancer Discov*. 2019;9(12):1736-1753.
6. Masetti R, Guidi V, Ronchini L, Bertuccio NS, Locatelli F, Pession A. The changing scenario of non-Down syndrome acute megakaryoblastic leukemia in children. *Crit Rev Oncol Hematol*. 2019;138:132-138.
7. Ma Z, Morris SW, Valentine V, et al. Fusion of two novel genes, RBM15 and MKL1, in the t(1;22)(p13;q13) of acute megakaryoblastic leukemia. *Nat Genet*. 2001;28(3):220-221.
8. Carroll A, Civin C, Schneider N, et al. The t(1;22) (p13;q13) is nonrandom and restricted to infants with acute megakaryoblastic leukemia: a Pediatric Oncology Group Study. *Blood*. 1991;78(3):748-752.
9. de Rooij JD, Branstetter C, Ma J, et al. Pediatric non-Down syndrome acute megakaryoblastic leukemia is characterized by distinct genomic subsets with varying outcomes. *Nat Genet*. 2017;49(3):451-456.
10. de Rooij JD, Hollink IH, Arentsen-Peters ST, et al. NUP98/JARID1A is a novel recurrent abnormality in pediatric acute megakaryoblastic leukemia with a distinct HOX gene expression pattern. *Leukemia*. 2013;27(12):2280-2288.
11. van Zutven LJ, Onen E, Velthuizen SC, et al. Identification of NUP98 abnormalities in acute leukemia: JARID1A (12p13) as a new partner gene. *Genes Chromosomes Cancer*. 2006;45(5):437-446.
12. Cardin S, Bilodeau M, Roussy M, et al. Human models of NUP98-KDM5A megakaryocytic leukemia in mice contribute to uncovering new biomarkers and therapeutic vulnerabilities. *Blood Adv*. 2019;3(21):3307-3321.
13. Roussy M, Bilodeau M, Jouan L, et al. NUP98-BPTF gene fusion identified in primary refractory acute megakaryoblastic leukemia of infancy. *Genes Chromosomes Cancer*. 2018;57(6):311-319.
14. Thiollier C, Lopez CK, Gerby B, et al. Characterization of novel genomic alterations and therapeutic approaches using acute megakaryoblastic leukemia xenograft models. *J Exp Med*. 2012;209(11):2017-2031.
15. Gruber TA, Larson Gedman A, Zhang J, et al. An Inv(16)(p13.3q24.3)-encoded CBFA2T3-GLIS2 fusion protein defines an aggressive subtype of pediatric acute megakaryoblastic leukemia. *Cancer Cell*. 2012;22(5):683-697.

16. Masetti R, Pigazzi M, Togni M, et al. CBFA2T3-GLIS2 fusion transcript is a novel common feature in pediatric, cytogenetically normal AML, not restricted to FAB M7 subtype. *Blood*. 2013;121(17):3469-3472.
17. Smith JL, Ries RE, Hylkema T, et al. Comprehensive Transcriptome Profiling of Cryptic CBFA2T3-GLIS2 Fusion-Positive AML Defines Novel Therapeutic Options: A COG and TARGET Pediatric AML Study. *Clin Cancer Res*. 2020;26(3):726-737.
18. Le Q, Hadland B, Smith JL, et al. CBFA2T3-GLIS2 model of pediatric acute megakaryoblastic leukemia identifies FOLR1 as a CAR T cell target. *J Clin Invest*. 2022;132(22).
19. Mercher T, Schwaller J. Pediatric Acute Myeloid Leukemia (AML): From Genes to Models Toward Targeted Therapeutic Intervention. *Front Pediatr*. 2019;7:401.
20. Li J, Kalev-Zylinska ML. Advances in molecular characterization of pediatric acute megakaryoblastic leukemia not associated with Down syndrome; impact on therapy development. *Front Cell Dev Biol*. 2023;11:1170622.
21. Chisholm KM, Smith J, Heerema-McKenney AE, et al. Pathologic, cytogenetic, and molecular features of acute myeloid leukemia with megakaryocytic differentiation: A report from the Children's Oncology Group. *Pediatr Blood Cancer*. 2023:e30251.
22. Fischer MA, Moreno-Miralles I, Hunt A, Chyla BJ, Hiebert SW. Myeloid translocation gene 16 is required for maintenance of haematopoietic stem cell quiescence. *EMBO J*. 2012;31(6):1494-1505.
23. Leung A, Ciau-Uitz A, Pinheiro P, et al. Uncoupling VEGFA functions in arteriogenesis and hematopoietic stem cell specification. *Dev Cell*. 2013;24(2):144-158.
24. Schuh AH, Tipping AJ, Clark AJ, et al. ETO-2 associates with SCL in erythroid cells and megakaryocytes and provides repressor functions in erythropoiesis. *Mol Cell Biol*. 2005;25(23):10235-10250.
25. Attanasio M, Uhlenhaut NH, Sousa VH, et al. Loss of GLIS2 causes nephronophthisis in humans and mice by increased apoptosis and fibrosis. *Nat Genet*. 2007;39(8):1018-1024.
26. Wen QJ, Yang Q, Goldenson B, et al. Targeting megakaryocytic-induced fibrosis in myeloproliferative neoplasms by AURKA inhibition. *Nat Med*. 2015;21(12):1473-1480.
27. Thirant C, Ignacimouttou C, Lopez CK, et al. ETO2-GLIS2 Hijacks Transcriptional Complexes to Drive Cellular Identity and Self-Renewal in Pediatric Acute Megakaryoblastic Leukemia. *Cancer Cell*. 2017;31(3):452-465.
28. Tang T, Le Q, Castro S, et al. Targeting FOLR1 in high-risk CBF2AT3-GLIS2 pediatric AML with STRO-002 FOLR1-antibody-drug conjugate. *Blood Adv*. 2022;6(22):5933-5937.
29. Drenberg CD, Shelat A, Dang J, et al. A high-throughput screen indicates gemcitabine and JAK inhibitors may be useful for treating pediatric AML. *Nat Commun*. 2019;10(1):2189.
30. Hanahan D, Weinberg RA. Hallmarks of cancer: the next generation. *Cell*. 2011;144(5):646-674.
31. Parry N, Wheadon H, Copland M. The application of BH3 mimetics in myeloid leukemias. *Cell Death Dis*. 2021;12(2):222.
32. Merino D, Kelly GL, Lessene G, Wei AH, Roberts AW, Strasser A. BH3-Mimetic Drugs: Blazing the Trail for New Cancer Medicines. *Cancer Cell*. 2018;34(6):879-891.
33. Delbridge AR, Grabow S, Strasser A, Vaux DL. Thirty years of BCL-2: translating cell death discoveries into novel cancer therapies. *Nat Rev Cancer*. 2016;16(2):99-109.

34. Singh R, Letai A, Sarosiek K. Regulation of apoptosis in health and disease: the balancing act of BCL-2 family proteins. *Nat Rev Mol Cell Biol*. 2019;20(3):175-193.
35. Strasser A, Vaux DL. Cell Death in the Origin and Treatment of Cancer. *Mol Cell*. 2020;78(6):1045-1054.
36. Pollyea DA, Amaya M, Strati P, Konopleva MY. Venetoclax for AML: changing the treatment paradigm. *Blood Adv*. 2019;3(24):4326-4335.
37. Place AE, Goldsmith K, Bourquin JP, et al. Accelerating drug development in pediatric cancer: a novel Phase I study design of venetoclax in relapsed/refractory malignancies. *Future Oncol*. 2018;14(21):2115-2129.
38. Pullarkat VA, Lacayo NJ, Jabbour E, et al. Venetoclax and Navitoclax in Combination with Chemotherapy in Patients with Relapsed or Refractory Acute Lymphoblastic Leukemia and Lymphoblastic Lymphoma. *Cancer Discov*. 2021;11(6):1440-1453.
39. Opferman JT, Kothari A. Anti-apoptotic BCL-2 family members in development. *Cell Death Differ*. 2018;25(1):37-45.
40. Kuusanmaki H, Leppa AM, Polonen P, et al. Phenotype-based drug screening reveals association between venetoclax response and differentiation stage in acute myeloid leukemia. *Haematologica*. 2020;105(3):708-720.
41. Chonghaile TN, Roderick JE, Glenfield C, et al. Maturation stage of T-cell acute lymphoblastic leukemia determines BCL-2 versus BCL-XL dependence and sensitivity to ABT-199. *Cancer Discov*. 2014;4(9):1074-1087.
42. Pei S, Pollyea DA, Gustafson A, et al. Monocytic Subclones Confer Resistance to Venetoclax-Based Therapy in Patients with Acute Myeloid Leukemia. *Cancer Discov*. 2020;10(4):536-551.
43. Aldoss I, Yang D, Pillai R, et al. Association of leukemia genetics with response to venetoclax and hypomethylating agents in relapsed/refractory acute myeloid leukemia. *Am J Hematol*. 2019;94(10):E253-E255.
44. DiNardo CD, Tiong IS, Quaglieri A, et al. Molecular patterns of response and treatment failure after frontline venetoclax combinations in older patients with AML. *Blood*. 2020;135(11):791-803.
45. Josefsson EC, James C, Henley KJ, et al. Megakaryocytes possess a functional intrinsic apoptosis pathway that must be restrained to survive and produce platelets. *J Exp Med*. 2011;208(10):2017-2031.
46. Mason KD, Carpinelli MR, Fletcher JI, et al. Programmed anuclear cell death delimits platelet life span. *Cell*. 2007;128(6):1173-1186.
47. Tse C, Shoemaker AR, Adickes J, et al. ABT-263: a potent and orally bioavailable Bcl-2 family inhibitor. *Cancer Res*. 2008;68(9):3421-3428.
48. Khan S, Zhang X, Lv D, et al. A selective BCL-XL PROTAC degrader achieves safe and potent antitumor activity. *Nat Med*. 2019;25(12):1938-1947.
49. Kuusanmaki H, Dufva O, Vaha-Koskela M, et al. Erythroid/megakaryocytic differentiation confers BCL-XL dependency and venetoclax resistance in acute myeloid leukemia. *Blood*. 2022.
50. Eidenschink Brodersen L, Alonzo TA, Menssen AJ, et al. A recurrent immunophenotype at diagnosis independently identifies high-risk pediatric acute myeloid leukemia: a report from Children's Oncology Group. *Leukemia*. 2016;30(10):2077-2080.

51. Ansari U, Tomellini E, Chagraoui J, et al. CEACAM1 is a novel culture-compatible surface marker of expanded long-term reconstituting hematopoietic stem cells. *Blood Adv*. 2022;6(12):3626-3631.
52. Aubert L, Nandagopal N, Steinhart Z, et al. Copper bioavailability is a KRAS-specific vulnerability in colorectal cancer. *Nat Commun*. 2020;11(1):3701.
53. Fares I, Chagraoui J, Lehnertz B, et al. EPCR expression marks UM171-expanded CD34(+) cord blood stem cells. *Blood*. 2017;129(25):3344-3351.
54. Fitter S, Tetaz TJ, Berndt MC, Ashman LK. Molecular cloning of cDNA encoding a novel platelet-endothelial cell tetra-span antigen, PETA-3. *Blood*. 1995;86(4):1348-1355.
55. Matsuo Y, Drexler HG, Kaneda K, et al. Megakaryoblastic leukemia cell line MOLM-16 derived from minimally differentiated acute leukemia with myeloid/NK precursor phenotype. *Leuk Res*. 2003;27(2):165-171.
56. Brodersen LE, Gerbing RB, Pardo ML, et al. Morphologic remission status is limited compared to DeltaN flow cytometry: a Children's Oncology Group AAML0531 report. *Blood Adv*. 2020;4(20):5050-5061.
57. Hay SB, Ferchen K, Chetal K, Grimes HL, Salomonis N. The Human Cell Atlas bone marrow single-cell interactive web portal. *Exp Hematol*. 2018;68:51-61.
58. van Galen P, Hovestadt V, Wadsworth Ii MH, et al. Single-Cell RNA-Seq Reveals AML Hierarchies Relevant to Disease Progression and Immunity. *Cell*. 2019;176(6):1265-1281 e1224.
59. Afreen S, Bohler S, Muller A, et al. BCL-XL expression is essential for human erythropoiesis and engraftment of hematopoietic stem cells. *Cell Death Dis*. 2020;11(1):8.
60. Debrincat MA, Josefsson EC, James C, et al. Mcl-1 and Bcl-x(L) coordinately regulate megakaryocyte survival. *Blood*. 2012;119(24):5850-5858.
61. Roberts AW. Therapeutic development and current uses of BCL-2 inhibition. *Hematology Am Soc Hematol Educ Program*. 2020;2020(1):1-9.
62. Aid Z, Robert E, Lopez CK, et al. High caspase 3 and vulnerability to dual BCL2 family inhibition define ETO2::GLIS2 pediatric leukemia. *Leukemia*. 2023;37(3):571-579.
63. Wunderlich M, Chen J, Sexton C, et al. PDX models of relapsed pediatric AML preserve global gene expression patterns and reveal therapeutic targets. *bioRxiv*. 2022:2022.2001.2031.478534.
64. Mishra AK, Mullanfiroze K, Chiesa R, Vora A. Azacitidine and venetoclax for post-transplant relapse in a case of CBFA2T3/GLIS2 childhood acute myeloid leukaemia. *Pediatr Blood Cancer*. 2021;68(11):e29221.
65. Karol SE, Alexander TB, Budhraja A, et al. Venetoclax in combination with cytarabine with or without idarubicin in children with relapsed or refractory acute myeloid leukaemia: a phase 1, dose-escalation study. *Lancet Oncol*. 2020;21(4):551-560.
66. Kaefer A, Yang J, Noertersheuser P, et al. Mechanism-based pharmacokinetic/pharmacodynamic meta-analysis of navitoclax (ABT-263) induced thrombocytopenia. *Cancer Chemother Pharmacol*. 2014;74(3):593-602.
67. Wilson WH, O'Connor OA, Czuczman MS, et al. Navitoclax, a targeted high-affinity inhibitor of BCL-2, in lymphoid malignancies: a phase 1 dose-escalation study of safety, pharmacokinetics, pharmacodynamics, and antitumour activity. *Lancet Oncol*. 2010;11(12):1149-1159.

FIGURE LEGENDS

Figure 1. Generation of human models of CBFA2T3::GLIS2 leukemia. A) Experimental procedure used to establish xenograft models of CBFA2T3::GLIS2 (CG2) acute megakaryoblastic leukemia (mCG2 AMKL) using independent lentiviral transduction in cord blood CD34+ cells (CB-CD34+, pool of 6 CB units) and transplantation in NSG recipient mice. **B**) Schematic representation of 6 CG2 leukemia models (mCG2) describing initial gene transfer (G.T., %GFP) at the time of transplantation and leukemia latency in primary recipient mice. Mouse identification in brackets. One of 10 mice was not available for analysis. **C)** Detection of CG2 fusion transcript expression by RT-PCR with RNA isolated from leukemic blasts, as indicated. M07e and normal lineage-depleted cord blood (CB-LIN-) cells were used as positive and negative control, respectively. *ABL1* was used as housekeeping gene. **D)** Percentage of infiltrating human blasts (hCD45+ GFP+) and **E**) CD41+ cells (of hCD45+ GFP+ population) in bone marrow (BM) and spleen of CG2 primary recipient mice (color code indicates distinct primary mice). **F**) Hematoxylin-phloxine-saffron-stained longitudinal sections of tibia bones harvested from primary recipient mice transplanted with control CB-CD34+ cells transduced with empty vector (left panel, 47 weeks after transplantation) and from a CG2-1 AMKL model (secondary recipient transplanted with 1 x 10^6 CG2-1 AMKL xenograft cells and sacrificed 11.1 weeks after transplantation, right panel). **G)** Survival curves of primary recipient mice transplanted with CB-CD34+ cells transduced with CG2 (black line) or empty vector (gray dashes), and mice serially transplanted up to 3 times with CG2-1 AMKL (red lines). Giemsa-stained cytospins and flow cytometry profiles of leukemic BM cells from representative (**H-I**) primary (1^{ary}) and (**J-K**) secondary (2^{ary}) CG2-1 AMKL recipient mice (2^{ary} recipient transplanted with 1.4 x 10^6 CG2-1 AMKL xenograft cells and sacrificed 6.9 weeks after

transplantation). Detailed characteristics of other CG2 leukemia xenografts in serially transplanted recipient mice are described in Table S5 and Suppl. Fig. S1 **L)** Survival curves of NSG recipient mice transplanted with CG2-1 AMKL xenograft cells in a limiting dilution cell transplantation assay and **M)** estimation of leukemia initiating cell (LIC) frequency and 95% confidence interval (red dashes) using the extreme limiting dilution analysis software (http://bioinf.wehi.edu.au/software/elda/).

Figure 2. Gene expression in CBFA2T3::GLIS2 leukemia models correlate with pediatric disease. A) Left panel, correlation of differential gene expression (log 2-fold change, L2FC) in CBFA2T3::GLIS2 (CG2) acute megakaryoblastic leukemia (AMKL) models and patients from our institutional dataset (CHUSJ) compared to a validation dataset of pediatric CG2 AMKL (St. Jude). Differentially expressed genes, defined as |L2FC>1| and FDR q-value < 0.05, common to both datasets are indicated in blue or orange and define the CG2 signature (Table S7). Institutional (Inst.) dataset: CG2 AMKL models (n=10) and CG2 patient samples (n=2) compared with NUP98::KDM5A (N5A) AMKL models (n=5), N5A patient samples (n=2) and normal CB-CD34^{+} cells (n=4). Validation (Val.) dataset: CG2 AMKL (n=12) vs other genetic subtypes of AMKL (n=61) from pediatric patients at diagnosis[9]. Right panel, upset plots showing differentially expressed genes that are jointly over- (n=399) or under-expressed (n=330) in CG2 leukemias, corresponding to blue and orange dots in A. **B)** Hierarchical clustering using the 729 differentially expressed genes of the CG2 gene expression signature. **C)** Heatmap showing protein (Log2 (MS intensity), left panels) and mRNA (RNAseq, FPKM values, right panels) expression of cell surface markers associated to CG2 leukemia (high expression in mCG2-1 and mCG2-2 leukemia models Log2(LC-MS values) ≥ 16 & RNAseq FPKM ≥ 5) and weak/no

expression in normal CB-CD34^{+}cells (Log2(LC-MS values) < 16 & RNAseq FPKM < 5). Samples were analyzed in triplicates and represented as mean expression (biological triplicates for RNAseq and technical triplicates for proteomic data). For comparison, values for mN5A and pdxNTF are shown alongside mCG2 samples. The St. Jude validation cohort RNAseq expression is presented as a separate column. **D)** Star plot presenting the p-adjusted values of differentially expressed genes and differentially expressed proteins (FDR < 0.05) (Transcriptome: CHUSJ CG2 vs N5A AMKL & normal CB-CD34+; Surfaceome: CG2 vs NUP98r & CB-CD34^{+}). The scores are calculated by multiplying the algebraic sign (+ or -) of the Log2 fold change, surfaceome or transcriptome, by the corresponding Log10(adjusted p-value). Significantly up-regulated CG2 AMKL-specific surface markers intersecting both datasets are labelled. **E)** Validation by flow cytometry of PCDH19 surface expression on CG2 AMKL cells from patient (pCG2-1), model mCG2-1, and M07e cell line. PCDH19 is not expressed on lineage-depleted human cord blood cells (CB-CD34+). Samples were co-stained with NCAM1. **F**) Left panels: scatter plot representations showing the best pairwise correlations of cell surface marker genes that select for CG2 genotype in a validation dataset of pediatric AMKL (out of 8 cell surface marker combinations, see Suppl. Fig. S13). Right panels: values, from top to bottom, represent the global and subtype-specific Kendall rank correlation coefficients. P-values: * <0.05, ** <0.005.

Figure 3. CBFA2T3::GLIS2 leukemia consist of immature mega-erythroid stem and progenitor lineages. A) UMAP of normal bone marrow lineages. The stem-mega-erythroid compartment is circled, relevant populations are labelled, and differentiation trajectories are

highlighted with arrows. **B**) Differentially expressed genes between cells of the megakaryocytic lineage (CD34+ MEP, CD34+ MKP, platelets) and all other cell types in normal bone marrow (Table S11). Genes relevant to the megakaryocytic differentiation are highlighted in red, genes of the mitochondrial apoptotic pathway are highlighted in blue. **C**) Percentage positive cells for each gene in synthetic models of CG2 (mCG2), patient (pCG2), other subtypes of AML and in specific populations of the normal bone marrow (HSC, MEP, MKP, PLT). The horizontal line represents the median of the group, the patient and models are color coded as in (D) and the normal samples are color coded based on donor as in (Suppl Fig. S14D). The bottom panel shows the *ITGA2B* (CD41) expression per cell on a UMAP representation of model mCG2-1, patient pCG2-1 and normal BM (extended samples in Suppl Fig. S15-S16). **D**) Radar plot (top) of lineage composition assessed by scRNAseq in CG2 AMKL models and pediatric patients, as compared to diverse phenotypic and genetic subtypes of adult AML. The detailed proportion of each cell type is presented as stacked bar plots (bottom). Color coding of populations is as depicted in (A). **E**) Representation as in (C) of terminal differentiation gene expression (extended samples in Suppl Fig. S15-S16). **F**) Differentially expressed genes in the CD34+ MKP from the CG2 models and patients compared to normal CD34+ MKP (Table S12). Selected markers are highlighted in red and genes of the mitochondrial apoptotic pathway are highlighted in blue. **G**) Representation as in (C) of *BCL2* and *BCL2L1* (BCL-X_L) expression. HSC, hematopoietic stem cells; MEP, megakaryocyte-erythroid progenitors; MKP, megakaryocyte progenitors; PLT, platelets; Log2FC, Log2 fold change.

Figure 4. CBFA2T3::GLIS2 and NUP98r AMKL xenografts are sensitive to induction of the intrinsic apoptotic pathway. A-B) Dose-response curves and half maximal inhibitory

concentrations (IC50, Table S13) determined for each indicated sample of AMKL or AML, submitted to a viability assay in presence of Venetoclax or Navitoclax. (Cell-Titer Glo, 6-day incubation, 4 replicates). Viability readout was normalised to DMSO controls for each sample. **C-D**) Apoptosis assessed by Annexin V staining and flow cytometry of AKML xenografts (mCG2, pdxNTF, mN5A, n=2 biological replicates for each cell type), ML2 (AML cell line, n=2), or normal CB-CD34+ cells (n=3) treated 72h in culture as triplicates with the indicated BH3 mimetics (123.5 nM, 370 nM and 10 μM) or DMSO. p-values: ** <0.005, *** <0.001, **** <0.0001. **E-F)** Mitochondrial superoxide production was assessed by MitoSox staining and flow cytometry of AMKL xenografts or normal CB-CD34+ cells, treated with the indicated BH3 mimetics or DMSO for 72h in culture in duplicates. Staurosporine (STS) was used as positive control at 1μM. CG2, CBFA2T3::GLIS2; N5A, NUP98::KDM5A; NTF, NUP98::BPTF; mAMKL, synthetic xenograft AMKL; mAML, synthetic xenograft AML: pdx, patient-derived xenograft, CB-CD34+, cord blood CD34+ cells.

Figure 5. AMKL xenografts depend on pro-survival protein BCL-X_L for survival.

A) RNAseq expression values (log2(FPKM)) of selected genes implicated in intrinsic apoptosis pathway in model and patient leukemias from our institutional dataset. **B**) Cross-validation of gene expression in a large and published dataset of pediatric acute megakaryoblastic leukemia [9]. **C)** Protein levels of BCL-X_L (left panel) and BCL2 (right panel) in AMKL xenograft cells or normal CB-CD34+ cells assessed by intracellular flow cytometry. **D)** Apoptosis, assessed by

Annexin V staining and flow cytometry, **E)** relative gene expression detected by qRT-PCR, and **F)** pro-survival protein levels quantified by flow cytometry, following shRNA-mediated knockdown (KD) of pro-survival BCL2-proteins (BCL-X_L, BCL2 and BCL-W) in CG2 xenografts (72h post-infection, 2 selected shRNA per gene). Samples were compared to non-transduced (NT) or cells infected with control shRNA against Renilla (shRenilla). See Suppl. Fig. S18 for KD studies in mCG2-2 cells. **G)** Dose response curves and IC50 values were determined after incubation of AMKL or AML xenografts with DT2216 (BCL-X_L PROTAC) or DMSO for 6d, followed by viability readout with Cell-Titer Glo. Viability readout was normalised against DMSO for each sample. **H)** Amount of apoptosis assessed by Annexin V staining and flow cytometry in AMKL xenografts or normal CB-CD34+ cells after 72h of incubation with DT2216 at 100nM or 1μM in comparison to cells treated with DMSO. CB-CD34+, cord blood CD34+ cells; CG2, CBFA2T3::GLIS2; PDX, patient-derived xenograft; NTF, NUP98::BPTF; N5A, NUP98::KDM5A; KMT2Ar, KMT2A rearranged; HOXr, HOX rearrangGATA1s, GATA1 truncation; RBM-MKL, RBM15::MKL1. P-values: * <0.05, ** <0.005, **** <0.0001. MFI, mean fluorescence intensity.

Figure 6: CBFA2T3::GLIS2 AMKL is impaired by Navitoclax and DT2216 treatment *in vivo*.

A) Workflow of experimental procedures to assess the *in vivo* activity of Navitoclax or DT2216 in CBFA2T3::GLS2 (mCG2-1) AMKL xenografts. At day of sacrifice **B) s**pleen weights **C)** percentage of leukemic blasts in peripheral blood (%GFP+hCD45+) and **D)** infiltration of the bone marrow (BM) and spleen (%GFP+ cells) was assessed in transplanted mice after treatment with either vehicle only (n=5) or Navitoclax (n=6) for 3 weeks. For comparison, spleen weights

of non-transplanted mice (n=6) were recorded for **B). E)** Hematoxylin-eosin stained (HE) longitudinal sections of tibia and spleen collected from mice at day of sacrifice. Conditions were either transplanted with CG2 but not treated (leukemic), transplanted and treated with vehicle only (Vehicle), not transplanted and not treated age-matched littermates of treatment groups (not transplanted) or transplanted and Navitoclax treated mice (Navitoclax). **F)** Leukemic burden (%GFP hCD45+) was monitored during treatment in the blood of vehicle and Navitoclax-treated mice. **G)** Kaplan-Meier survival curves of mCG2-1 transplanted mice treated either with vehicle or Navitoclax. Log-rank Mantel-Cox test was used to determine survival benefit. **H)** Leukemic burden (GFP+hCD45+) was monitored by bleeding in mCG2-1 vehicle-treated mice versus DT2216-treated ones. **I**) Kaplan-Meier survival curves of mCG2-1 AMKL model treated either with vehicle or DT2216. Survival benefit was determined with Log-rank Mantel-Cox test. P-values: * <0.05, ** < 0.005, *** < 0.001, **** < 0.0001.

Figure 7: Combinatorial use of BCL-X_L inhibitors and cytarabine demonstrates greater reduction of leukemic burden *in vivo* as compared to single agent treatment.

A) Dose-response curves and half maximal inhibitory concentrations (IC50, Table S13) determined for all six samples of CG2 AMKL, submitted to a viability assay in presence of cytarabine. (Cell-Titer Glo, 6-day incubation, 4 replicates). Viability readout was normalised to DMSO controls for each sample. **B)** Schematic overview of experimental design of combinatory treatments of xenotransplanted mice with Navitoclax and cytarabine (AraC). **C)** Percentage of leukemic blasts in peripheral blood (%GFP+hCD45+, left graph), infiltration of bone marrow (BM, middle graph) and spleen (right graph) was assessed in transplanted mice after 3 weeks of

indicated treatments. **D)** Percentage infiltration (%GFP+hCD45+) in the bone marrow of xenotransplanted and treated mice was compared at endpoint between matched Vehicle controls and mice either treated with DT2216 or Navitoclax, **E)** as well as their respective combinations with cytarabine (AraC).

Figure 1

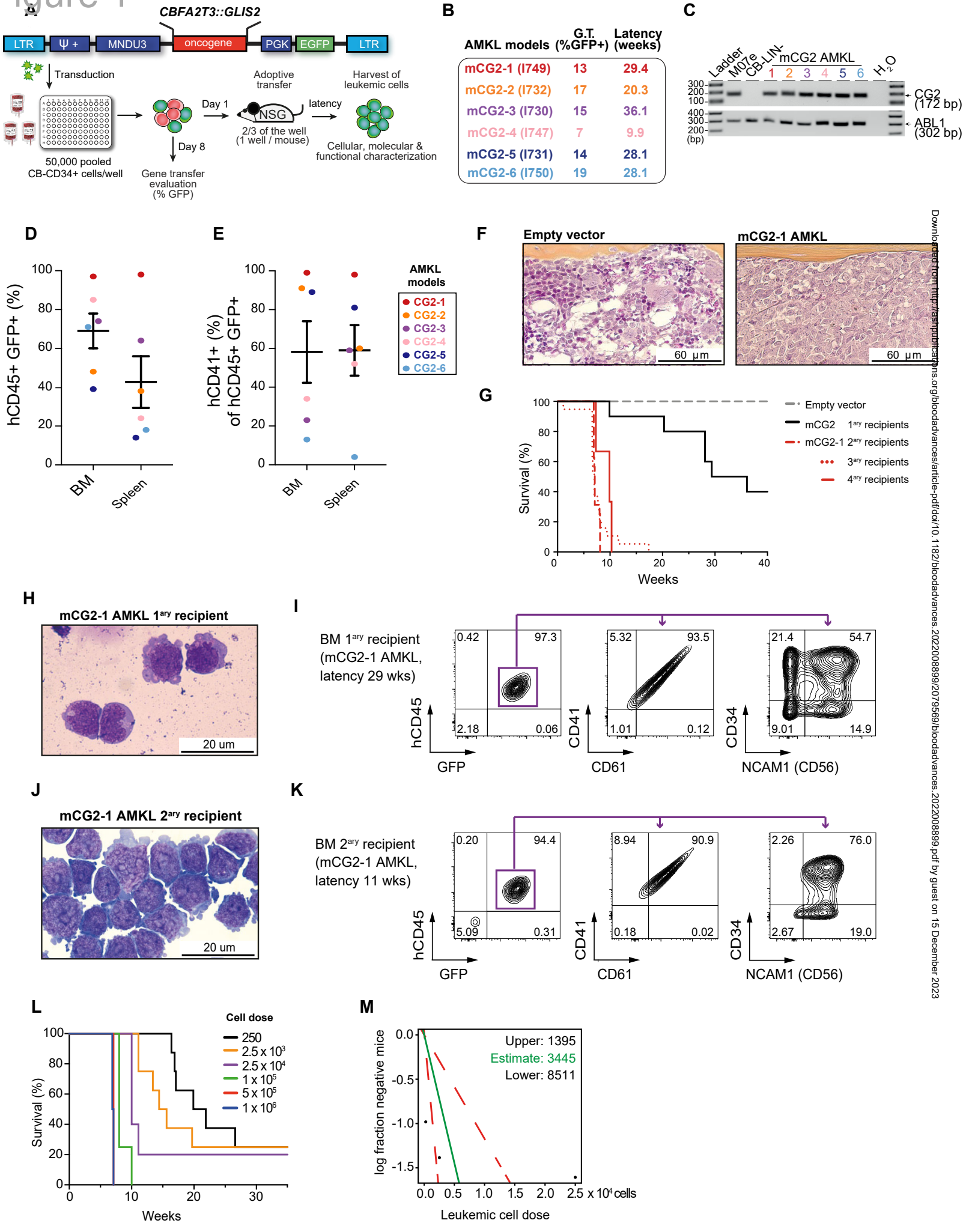

Figure 2

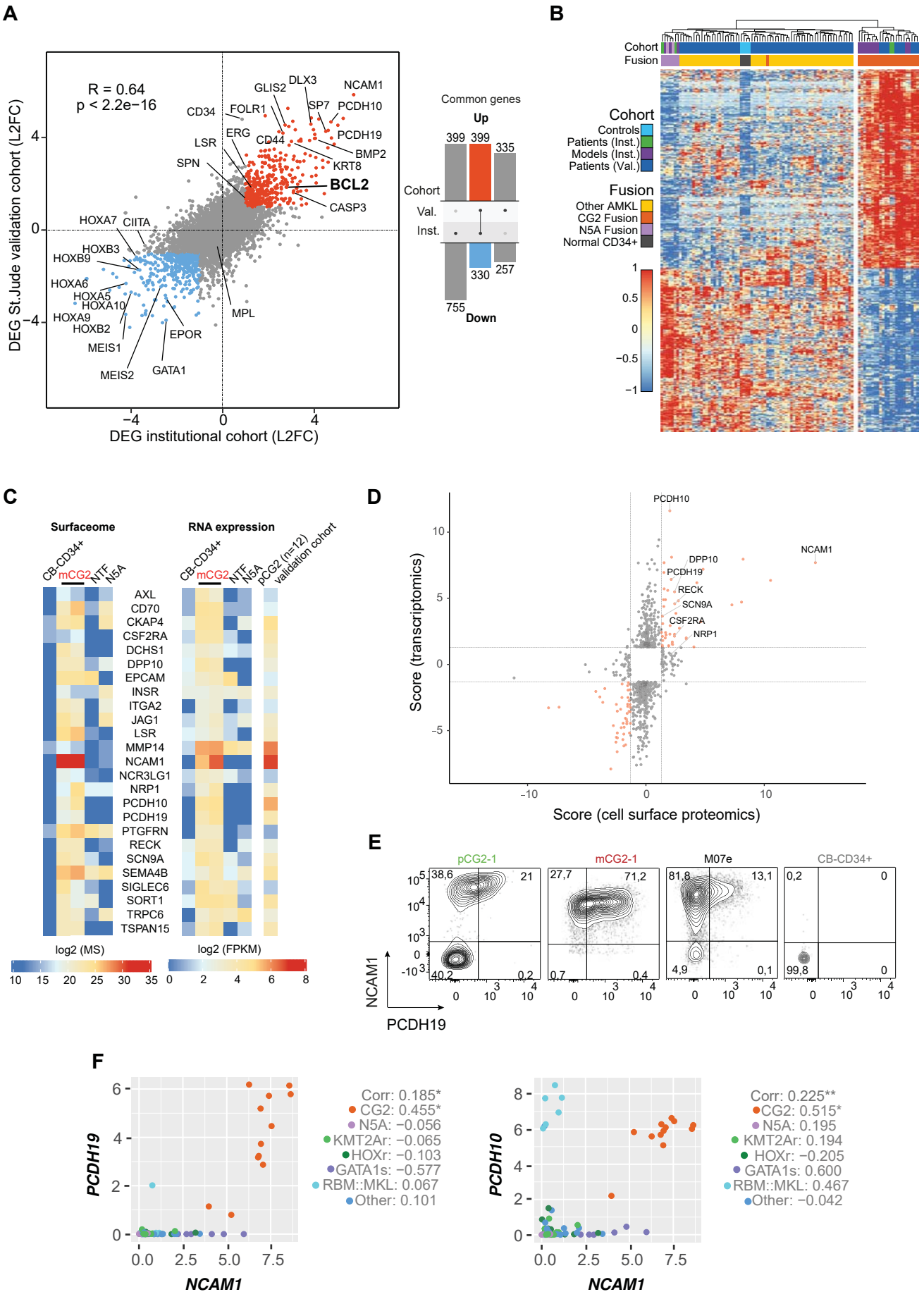

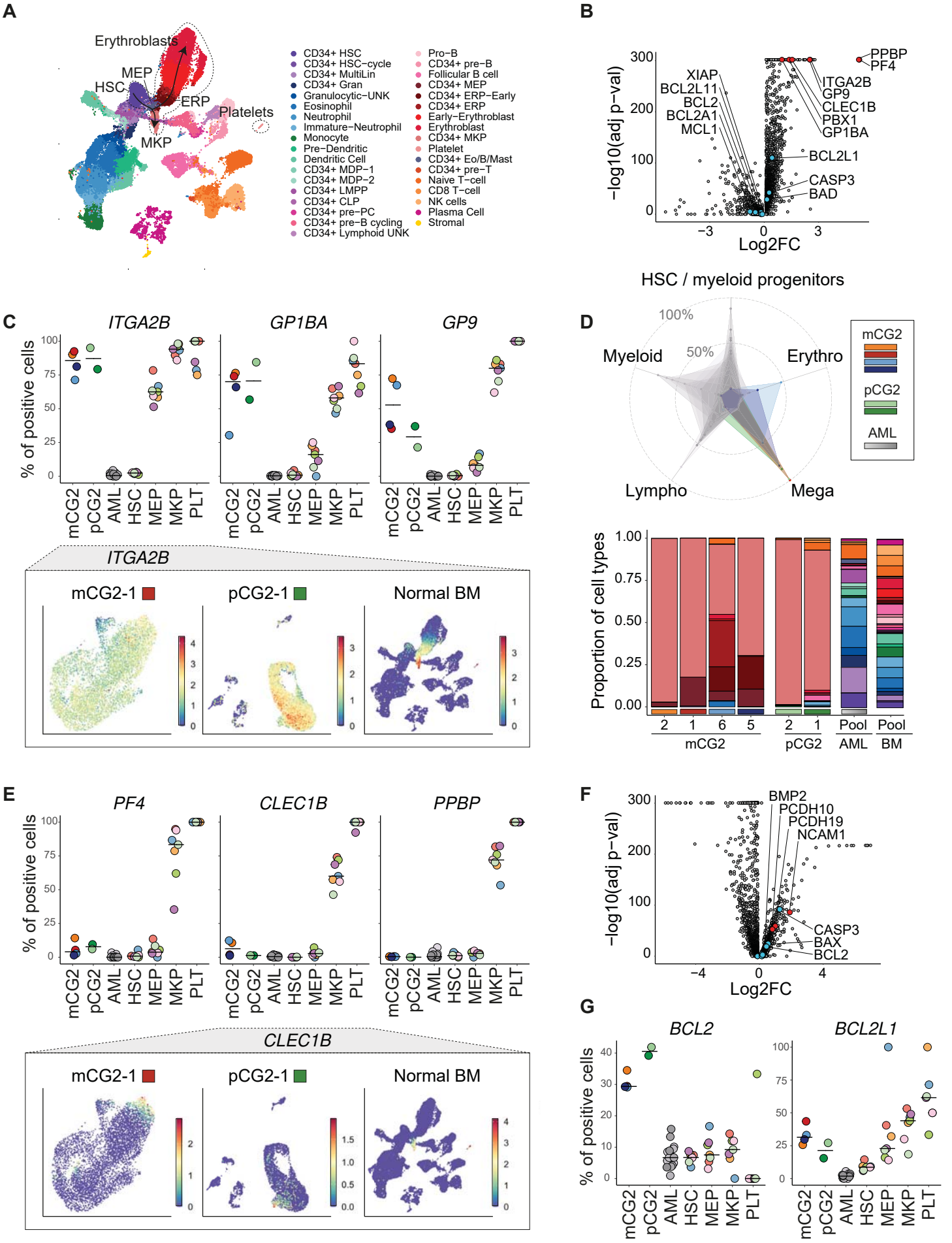

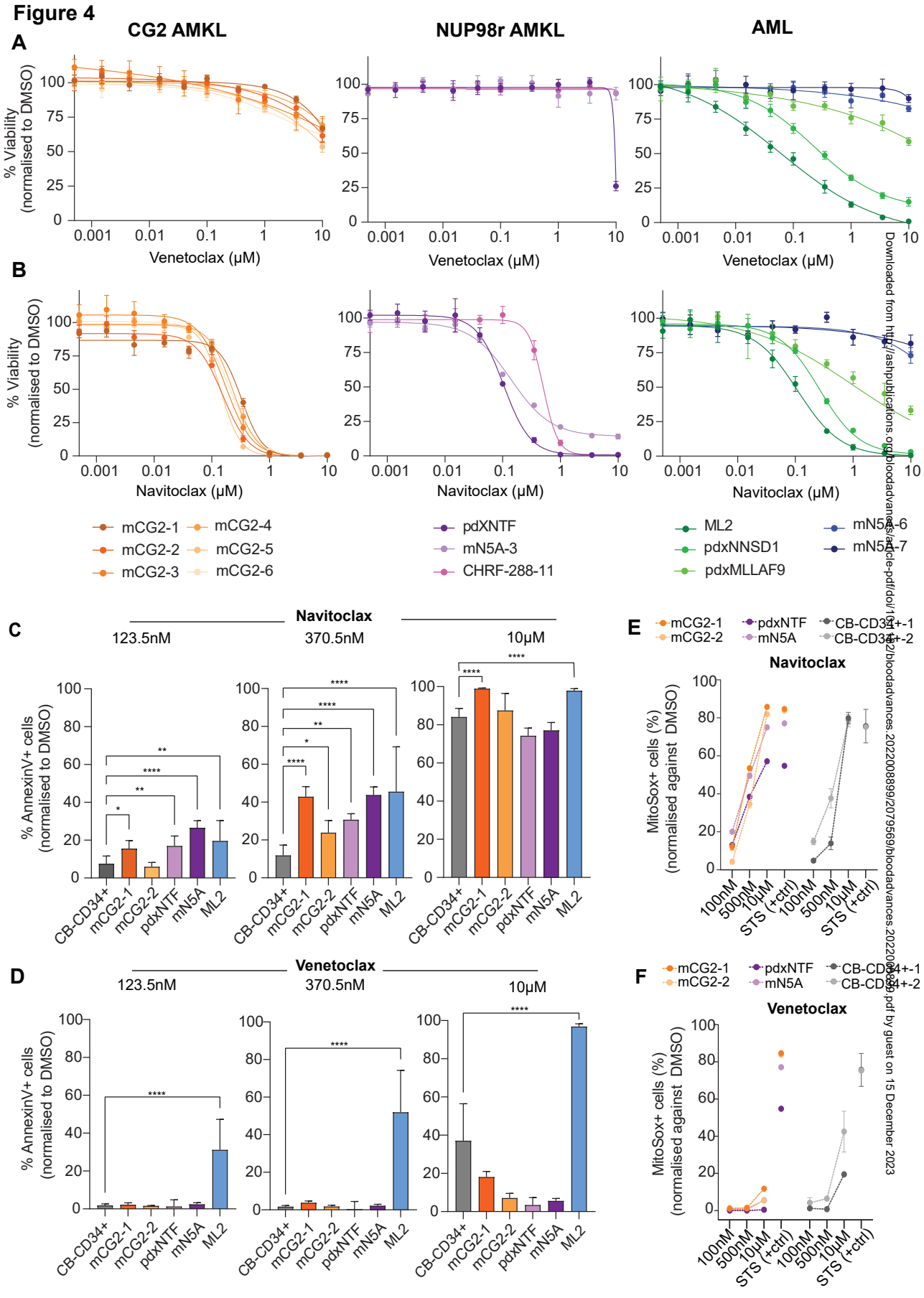

Figure 5

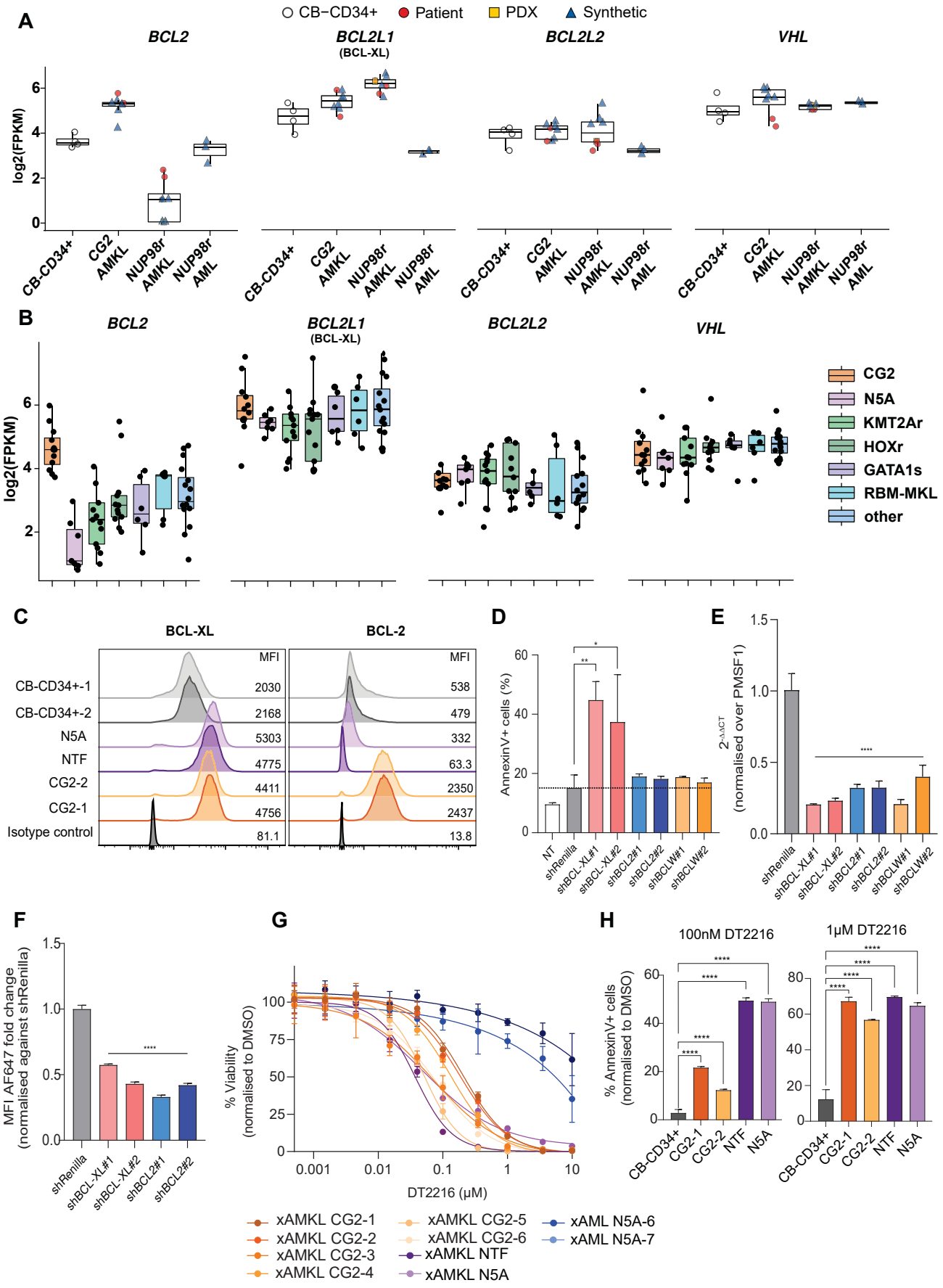

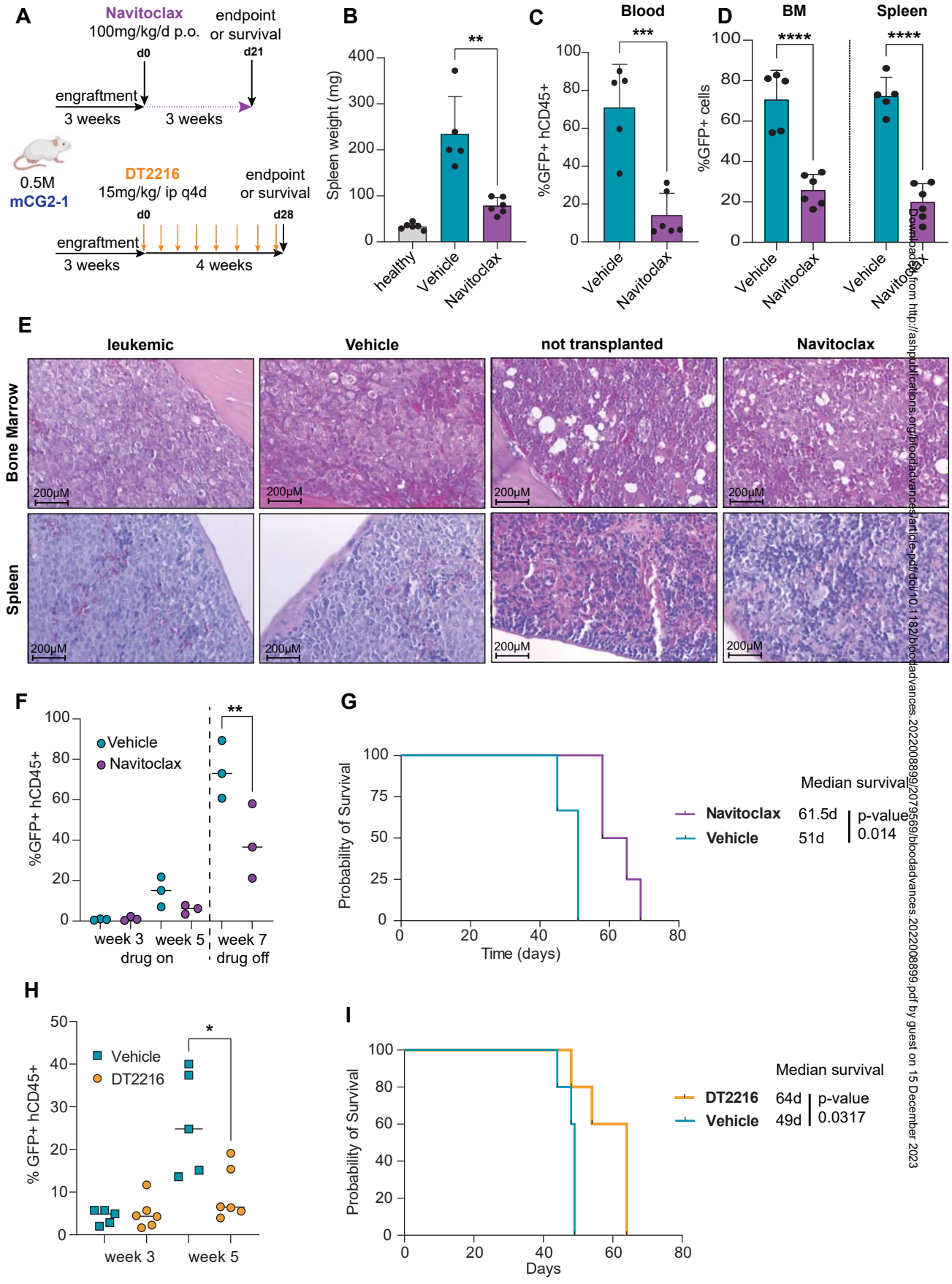

Figure 7